Raman Spectra of Shock Compressed Pentaerythritol Tetranitrate Single Crystals: Anisotropic Response

ARTICLE *in* THE JOURNAL OF PHYSICAL CHEMISTRY B · NOVEMBER 2006

Impact Factor: 3.3 · DOI: 10.1021/jp0680589 · Source: PubMed

Raman Spectra of Shock Compressed Pentaerythritol Tetranitrate Single Crystals: Anisotropic Response

N. Hemmi, Z. A. Dreger,* Y. A. Gruzdkov, J. M. Winey, and Y. M. Gupta

Institute for Shock Physics and Department of Physics, Washington State University, Pullman, Washington 99164-2816

Received: May 30, 2006

To gain insight into the anisotropic sensitivity of shocked pentaerythritol tetranitrate (PETN) single crystals, single-pulse Raman spectroscopy was used to examine the response of crystals shocked along the [100] (insensitive) and [110] (sensitive) orientations. High-resolution Raman spectra revealed several orientation-dependent features under shock compression: (i) substantially different stress dependence of the Raman shift for the CH_2 and NO_2 stretching modes for the two orientations, (ii) discontinuity in the stress dependence of the Raman shift for the CH_2 stretching modes above 4 GPa for the [110] orientation, and (iii) large broadening for the CH_2 and NO_2 asymmetric stretching modes for stresses above 4 GPa for the [110] orientation. The present data in combination with previous static pressure results provide support for conformational changes in PETN molecules for shock compression along the [110] (sensitive) orientation. Implications of the present results for the anisotropic sensitivity of shocked PETN are discussed.

I. Introduction

Pentaerythritol tetranitrate (PETN, $C(CH_2ONO_2)_4$) is an energetic crystal used extensively as an initiating or booster high explosive. It is well-established[1,2] that shock initiation of PETN single crystals is strongly anisotropic, and the shock-to-detonation transition (SDT) features depend markedly on the crystal orientation being compressed. Subsequently, a number of studies[3−7] have been undertaken in an attempt to understand the anisotropic sensitivity of shocked PETN.

Dick and co-workers[2,3] have attempted to relate the observed anisotropic sensitivity to the anisotropic mechanical response of shocked PETN. They proposed that the mechanical anisotropy is due to differences in the dislocation slip systems activated when the crystal is subjected to shock wave compression along different orientations. Furthermore, they suggested that shear deformation on the slip system depended on steric hindrance or resistance to molecular motion on either side of the slip interface; shock compression along the [110] (sensitive) orientation resulted in significant steric hindrance, while compression along the [100] (insensitive) orientation did not result in steric hindrance.[3] However, they did not offer any specific mechanism for initiation chemistry.

To address this need, Gruzdkov and Gupta proposed a model that linked mechanical anisotropy to initiation chemistry.[6] In this model, the steric hindrance concept was related, through shear deformation at the lattice level, to rotational conformations of PETN molecules.[6] Moreover, they proposed that conformational changes could lead to local lattice polarization and consequently to ionic reactions. The applicability of an ionic decomposition mechanism for shocked PETN crystals was examined using time-resolved electronic spectroscopy.[7] From the results of emission spectroscopy experiments, the nitronium ion (NO_2^+) was identified as a decomposition intermediate, and a four-step chemical initiation mechanism was proposed for shocked PETN that was consistent with an ionic decomposition process.[7]

According to the molecular hypothesis in ref 6, the difference between sensitive and insensitive orientations is that in the former the hindered shear produces local lattice polarization close to the shear planes, while in the latter, the unhindered shear does not. Thus, changes in rotational conformations of PETN molecules are central to this mechanism. The propensity of PETN to conformational changes was examined theoretically[6,8] and experimentally.[8,9] A number of stable conformers, corresponding to different molecular point symmetries, were identified using semiempirical calculations.[6,8] Additionally, density functional theory (DFT) calculations indicated that changes in conformation/symmetry of PETN molecules could be examined through changes in the vibrational spectrum.[8,10] Subsequently, Raman measurements identified two instances of symmetry/conformation changes: one under static high-pressure compression of crystals[8,9] and the other upon dissolving PETN in a polar solvent.[8] However, measurements of vibrational spectra in shocked PETN remain an important scientific need.

The work presented here represents, to the best of our knowledge, the first attempt to obtain vibrational spectra of HE crystals shocked along different orientations. Such data are needed to examine changes at the molecular level including conformation changes in shocked PETN. We used Raman spectroscopy, because it is efficient for distinguishing between different PETN conformers at ambient and high-pressure conditions.[8,9] Although Raman spectroscopy, in various forms, has been used before to examine the shock response of condensed materials (e.g., refs 11−15), previous methods were deemed unsuitable for providing the high spectral resolution data needed to discern changes in Raman spectra in shocked PETN. Additionally, because PETN emits light under shock loading,[2,5,7,16] the experimental method must provide an efficient rejection of background light. To meet these requirements, we developed a single pulse laser Raman method applicable for shock compression experiments. Here, we present Raman data

* Corresponding author. Email: dreger@wsu.edu.

10.1021/jp0680589 CCC: $33.50
Published on Web 09/26/2006

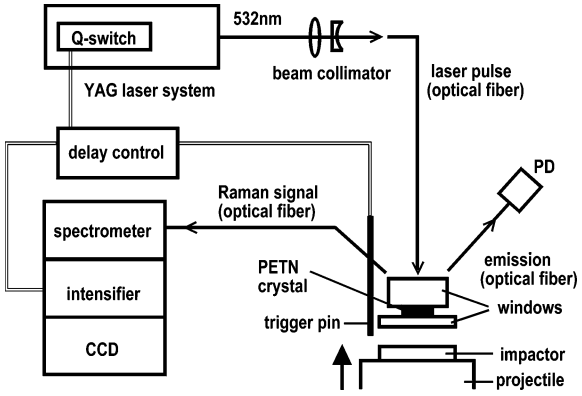

Figure 1. Schematic view of the experimental configuration. A 532-nm wavelength single pulse from a Nd:YAG laser is used for Raman excitation. The excitation pulse is synchronized with the shock event, and the Raman scattered light is recorded using the spectrometer−intensifier−CCD detection system. Shock-induced light emission is detected using a fast photodiode (PD). Solid lines with open arrows represent light propagation directions; double lines are electrical connections.

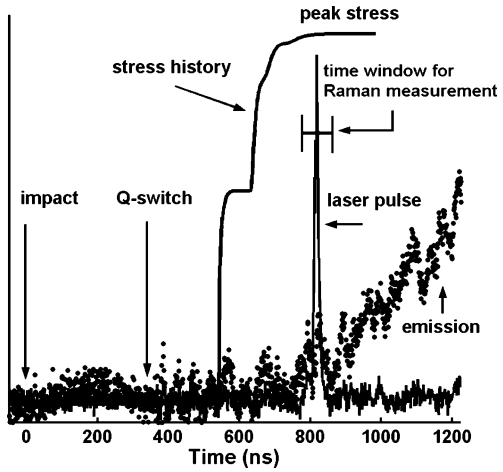

Figure 2. Time synchronization for acquisition of Raman spectra. The laser pulse is controlled by a Q-switch triggered by the projectile impact. The Raman spectrum is acquired after the PETN sample reaches the desired peak stress. The stress history curve illustrated by the solid line was calculated using a finite difference wave code (ref 18). The points represent the time profile for shock-induced light emission.

using this method to examine spectral changes in shocked PETN single crystals.

Specifically, this work had two objectives: (i) to examine changes in the vibrational spectra of PETN crystals shocked along [100] (insensitive) and [110] (sensitive) orientations and (ii) to determine if conformational changes, such as those proposed by Gruzdkov and Gupta,[6] can be observed in shocked PETN.

The remainder of this paper is organized as follows. The experimental methods are summarized briefly in the next section. Section III presents experimental results and their analysis. The results are discussed in section IV, and our main findings are summarized in section V.

II. Experimental Methods

All experiments were performed on PETN single crystals grown at the Los Alamos National Laboratory and provided to us by Dr. J. J. Dick. Samples with ∼8 × 8 mm^2 lateral dimensions oriented along the [100] or [110] direction were ground to ∼400-μm thickness and then polished to an optical finish using 0.3-μm aluminum oxide lapping sheets. The PETN samples were sandwiched between two *Z*-cut quartz windows, with liquid glycerol (spectroscopy grade, Aldrich Chemical) used to fill the gaps between the sample and the windows. The front and back windows were 3.5 mm and 9 mm thick, respectively.

A schematic diagram of the experimental setup is shown in Figure 1. A frequency-doubled Nd:YAG laser (532 nm), with 10-mJ energy per pulse and 20-ns pulse length, was used as the Raman excitation source. A single laser pulse was extracted from the 5-Hz pulse train and coupled into an optical fiber. The light from the optical fiber was focused to a 600-μm-diameter spot on the PETN sample. The backscattered light was collected using a 600-μm core diameter optical fiber and delivered into a spectrometer, where the elastically scattered excitation light at 532 nm was suppressed by a notch filter. The wavelength-dispersed light from the spectrometer was amplified by an image intensifier and recorded on a back-illuminated CCD. The overall spectral resolution of the system was about 3.5 cm^{-1}, which is significantly higher than in our previous work.[13]

Planar shock waves were generated by impacting projectiles, launched using a single-stage light-gas gun,[17] on to the target assembly. To achieve the desired final stress, the impactor plates were either *a*-cut sapphire or *Z*-cut quartz, or PMMA (poly-(methyl methacrylate)). Upon impact, a plane shock wave propagated through the front window and into the PETN sample. The sequence of events occurring after impact is illustrated in Figure 2. Reverberation of the shock wave between the front and back windows brought the PETN sample to the peak stress through a stepwise loading process. The final or peak stress is accurately known in our experiments, because it is determined by the impact velocity, impactor properties, and window material properties;[7] all of these are known quantities. Stress histories in PETN crystals were calculated using a wave propagation code.[18] To minimize the background light due to shock-induced emission,[7] the CCD was gated for 60 ns and the laser pulse was synchronized to arrive at the PETN sample during this time window, after the sample reached the desired peak stress. Details of the experimental method will be published elsewhere.[19]

TABLE 1: Summary of Shock Experiments

no.	spectral range (cm^{-1})	crystal orientation	sample thickness (μm)	impactor	projectile velocity (Km/s)	final stress (GPa)
1	800−1700	[100]	360	quartz	0.457	4.01
2	800−1700	[110]	385	quartz	0.461	4.05
3	800−1700	[100]	400	quartz	0.618	5.52
4	800−1700	[110]	410	quartz	0.616	5.50
5	800−1700	[100]	395	sapphire	0.504	6.50
6	800−1700	[110]	390	sapphire	0.507	6.54
7	2400−3300	[110]	400	PMMA	0.705	2.35
8	2400−3300	[100]	375	quartz	0.458	4.02
9	2400−3300	[110]	390	quartz	0.460	4.04
10	2400−3300	[100]	400	quartz	0.619	5.52
11	2400−3300	[110]	400	quartz	0.616	5.50
12	2400−3300	[100]	405	sapphire	0.499	6.43
13	2400−3300	[110]	385	sapphire	0.501	6.49

III. Results and Analysis

Single-pulse Raman spectra of shocked PETN single crystals were measured for several peak stresses up to 6.5 GPa. A total of 13 Raman experiments were performed, and relevant experimental details are summarized in Table 1. Selected spectra for both orientations are shown in Figures 3 and 4. Figure 3 shows Raman spectra in the frequency range 2800−3200 cm^{-1}, characteristic of strong CH_2 stretching modes. Figure 4 shows Raman spectra in the frequency range 800−1700 cm^{-1}, where

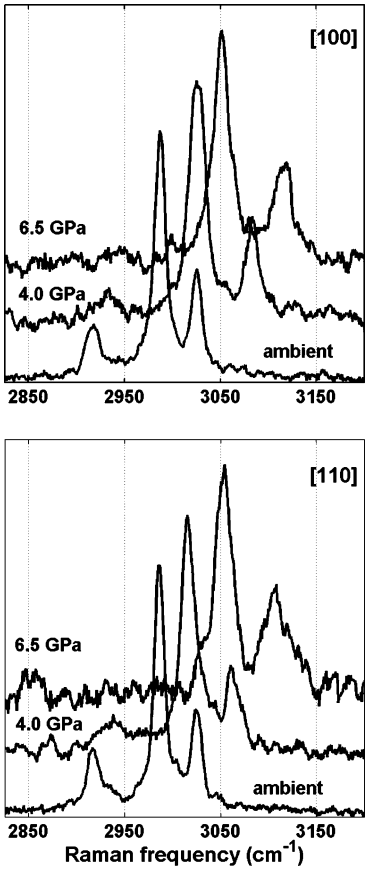

Figure 3. Raman spectra in the 2800−3200 cm^{-1} frequency range at several stresses for the [100] and [110] orientations. Three modes can be clearly resolved in this range: the CH_2 symmetric stretching mode at 2987 cm^{-1}, and two CH_2 asymmetric stretching modes at 2918 and 3026 cm^{-1}.

Raman modes associated with the NO_2 stretch and CH_2 bend and several modes associated with motions of the CCCON skeleton unit arm were observed (for the molecular geometry, see Figure 5). Mode assignments, presented in Table 2, are based on ref 10; assignments correspond to ambient conditions. However, not all of these mode peaks were visible under shock loading due to an increase in the background noise and broadening of some peaks. Although we employed a short time window for detection (60 ns) and a narrow range of spectral coverage (about 30 nm around 580 nm), the emission arising from the onset of shock-induced decomposition[7] was unavoidable and constituted the main source of the background increase. As seen in Figure 2, a photodiode signal, integrated over wavelengths greater than 550 nm, indicates that emission for the 6.5 GPa case started about 200 ns after the shock entered the sample, which was 50 ns before the laser pulse arrived at the PETN sample. Due to this emission, the increase in the spectral baseline at 6.5 GPa was more than twice that observed at 4.0 GPa. At stresses higher than 4.0 GPa, the background increase further degraded the signal-to-noise ratio. In the following paragraphs, we discuss Raman peaks discernible over the 0−6.5 GPa stress range for shocks along the [100] and [110] orientations.

In Figure 3, three CH_2 stretching modes were well-resolved at 2918, 2987, and 3026 cm^{-1} at ambient conditions. Under shock compression, a stress-induced frequency increase was clearly observed for the symmetric 2987 cm^{-1} and asymmetric 3026 cm^{-1} modes, while the weak asymmetric 2917 cm^{-1} mode became indistinguishable from the background above 4 GPa. The peaks for these CH_2 stretching modes were broadened

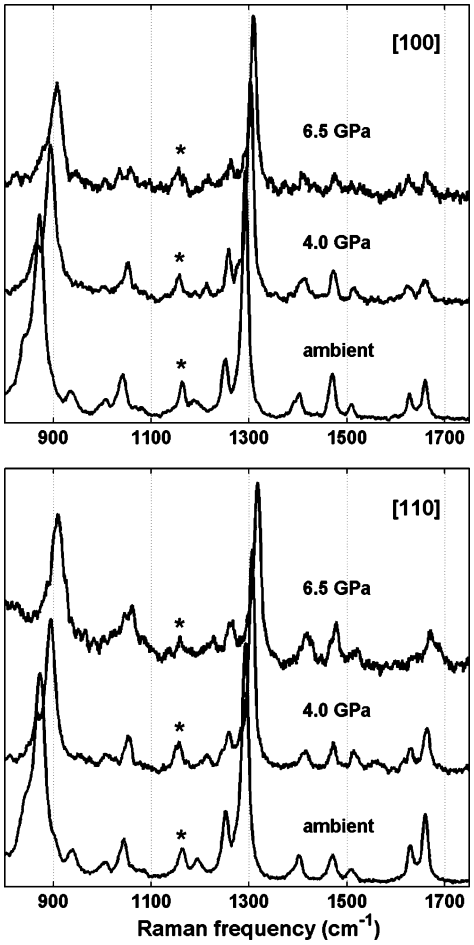

Figure 4. Raman spectra in the 800−1700 cm^{-1} frequency range at several stresses for the [100] and [110] orientations. The assignment of peaks is presented in Table 2. Two strong peaks at 873 and 1293 cm^{-1} correspond to the ON + CC stretching mode and the NO_2 symmetric stretching mode, respectively. The peak at 1163 cm^{-1}, denoted by an asterisk, is due to Raman scattering from the quartz window (ref 20).

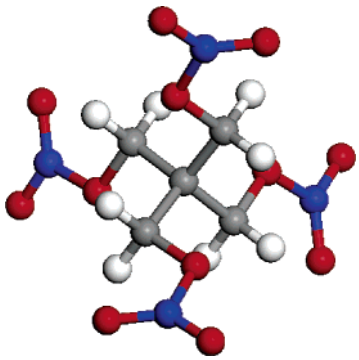

Figure 5. Equilibrium geometry of the PETN molecule in the crystal. Legend: carbon, grey; nitrogen, blue; oxygen, red; hydrogen, white.

substantially—especially for the asymmetric stretch. Despite uncertainties in the broadening determinations due to nonsymmetric broadening profiles and background fluctuations, it is clear that at 6.5 GPa the asymmetric 3026 cm^{-1} mode exhibited a substantially larger broadening for the [110] orientation when compared to the [100] orientation. Additionally, a small peak appeared on the lower frequency side of the symmetric 2987 cm^{-1} mode for the [110] orientation.

In Figure 4, frequency changes for all discernible Raman modes in the 800−1700 cm^{-1} range are displayed. These

TABLE 2: Raman Frequencies of Selected Modes for PETN Single Crystals at Ambient Conditions

frequency (cm^{-1})	assignment (ref 10)	symmetry (ref 10)
3026	CH_2 asymmetric stretch	E
2987	CH_2 symmetric stretch	A
2918	CH_2 asymmetric stretch	B
1661	NO_2 asymmetric stretch	A
1631	NO_2 asymmetric stretch	A
1514	CH_2 scissor	B
1473	CH_2 scissor	E
1403	CH_2 wag	A
1293	NO_2 symmetric stretch + CH_2 wag	A
1252	CH_2 bend	A
1194	CCC deformation + CH_2 wag	E
1043	CH_2 torsion + CCC deformation	A
1004	CO stretch + CCC deformation	E
939	CH_2 torsion + CCC deformation	E
873	ON stretch + CC stretch	A

changes were smaller than changes for the CH_2 stretching modes. The stretching modes of NO_2 functional groups, which are on the periphery of the PETN molecule, are of primary interest in this frequency region. A strong NO_2 symmetric stretching mode and two NO_2 asymmetric stretching modes are located at 1293, 1633, and 1661 cm^{-1}, respectively, at ambient conditions. The NO_2 symmetric stretching 1293 cm^{-1} mode yielded a substantial frequency shift with stress. In contrast, the asymmetric stretching modes showed comparatively smaller shifts that were accompanied by considerable broadening of the peaks. Similar to the CH_2 asymmetric stretching modes, both NO_2 asymmetric stretching modes showed larger broadening for the [110] orientation when compared to the [100] orientation at 6.5 GPa. In particular, the broadening of the 1633 cm^{-1} mode was so large that this peak ultimately merged into the baseline noise.

The other Raman peaks resolved at ambient conditions (see Figure 4) are from vibrational modes that involve combinations of different functional groups as shown in Table 2. Most of these peaks showed a low Raman intensity. However, the ON + CC arm stretching mode (873 cm^{-1}) had a large intensity and displayed a clear stress-induced frequency increase.

To examine the frequency shifts in detail, Gaussian functions were used to fit the Raman peaks for shock stresses up to 6.5 GPa. The uncertainty in the shifts of the Raman peaks was determined from a statistical average of three independent errors: spectral resolution of the detection system, uncertainties in calibration spectra, and standard error in Gaussian fitting.

As expected from inspection of the spectra in Figures 3 and 4, all analyzed Raman modes showed an increase in frequency under stress. For many of the modes, no apparent orientation dependence in the slope of the frequency shifts was observed; as an example, the plot for the ON + CC stretching mode is shown in Figure 6. However, examination of NO_2 and CH_2 stretching modes revealed interesting orientation dependences. As shown in Figure 7, the NO_2 symmetric stretching mode exhibited a clear difference in the slope of the frequency shifts between the two orientations: 3.4 ± 0.3 cm^{-1}/GPa for the [110] orientation and 2.4 ± 0.3 cm^{-1}/GPa for the [100] orientation, with linear shifts for both orientations. For the NO_2 asymmetric stretching modes, despite significant uncertainties due to low intensities and small shifts, a frequency shift of 8−10 cm^{-1} was found at 6.5 GPa for the [110] orientation, whereas little change from the ambient condition was observed for the [100] orientation.

For the CH_2 stretching modes, Voigt functions were used in fitting the 6.5 GPa spectra to improve the quality of the fit in the tail regions of the peaks, as shown in Figure 8. However, the positions of the main peaks were insensitive to whether Gaussian functions or Voigt functions were used. The CH_2 stretching modes show a considerable difference in the peak shapes between the two orientations. For the [100] orientation, two Voigt functions are sufficient to fit the spectral profile of the CH_2 symmetric and asymmetric stretching modes. However, the spectrum for the [110] orientation cannot be fitted with two functions. The bottom panel of Figure 8 clearly shows that additional spectral components are needed to properly fit the data. The need for additional components suggests that the anomalous broadening of the CH_2 stretching modes for the [110] orientation is due to the appearance of new spectral contributions, likely caused by the splitting of existing peaks.

In Figure 9, frequency shifts are plotted as a function of stress for the CH_2 symmetric 2987 cm^{-1} mode and the asymmetric 3026 cm^{-1} mode. It is evident that the stress dependence of the shifts is substantially different for the two orientations. For the [100] orientation, the frequency shifts for these two modes are nearly linear with stress, as illustrated by the solid lines in the figure. In contrast, for the [110] orientation, a discontinuous change in the slope of the frequency shifts was observed between 4 and 5.5 GPa. Up to 4 GPa, both modes exhibited a

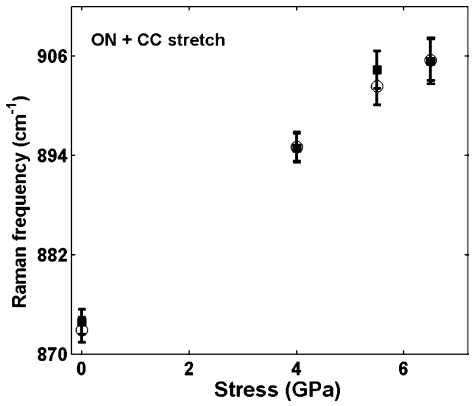

Figure 6. Stress dependence of the Raman frequency for the ON + CC stretching mode, 873 cm^{-1}, for the [100] orientation (open circles) and the [110] orientation (solid squares). Estimated error bars are also shown.

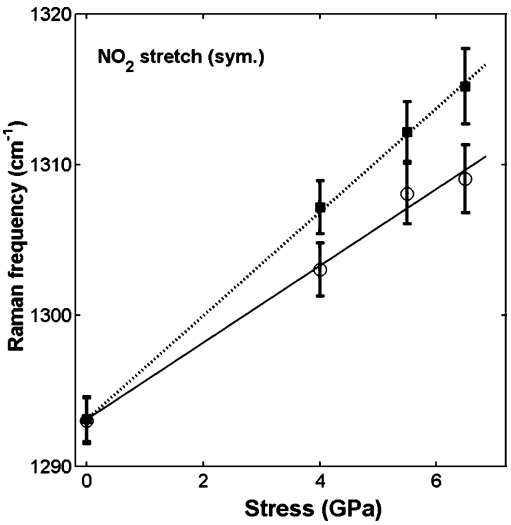

Figure 7. Stress dependence of the Raman frequency for the NO_2 symmetric stretching mode, 1293 cm^{-1}, for the [100] orientation (open circles) and the [110] orientation (solid squares). The solid and dotted lines are used to indicate shifts with stress for the [100] and [110] orientations, respectively. Estimated error bars are also shown.

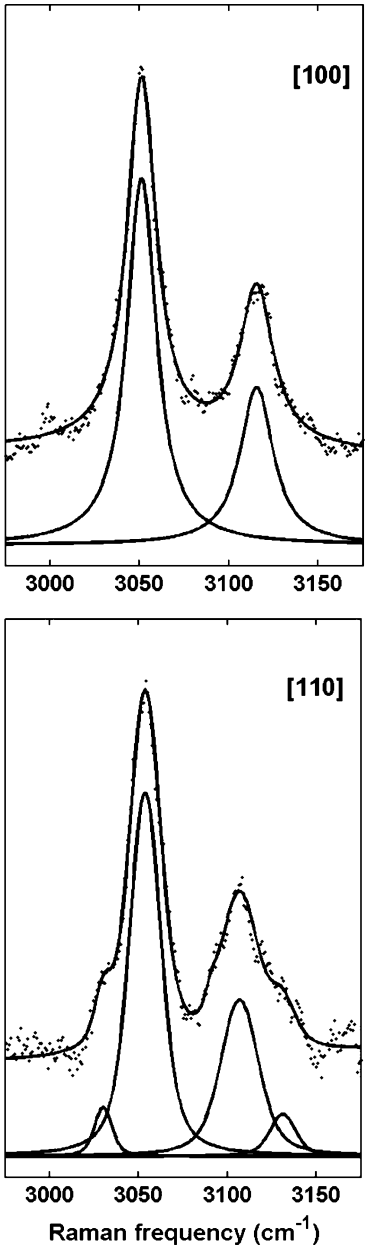

Figure 8. Peak fitting analysis for the CH_2 stretching modes. The points are the experimental data. Solid lines represent Voigt functions for fitting peaks for the [100] and [110] orientations. For the [110] orientation, additional peaks are required to obtain an adequate fit.

somewhat smaller slope for the [110] orientation compared to the [100] orientation. However, at higher stresses, a similar slope was observed for both orientations. This discontinuous behavior in slope was more pronounced for the asymmetric 3026 cm^{-1} mode than for the symmetric 2987 cm^{-1} mode. Also, the two peaks, corresponding to the shoulders in the [110] data in Figure 8, are plotted as crosses in Figure 9.

IV. Discussion

Our Raman spectroscopy results indicate a clear orientation dependence in the shock compression response of PETN crystals. This dependence is manifested primarily in the following features: (i) the slope of the Raman shift as a function of shock stress for the CH_2 and NO_2 stretching modes is substantially different for the [100] and [110] orientations (Figures 7 and 9), (ii) a discontinuity in the slope of the Raman shift versus stress plot for the CH_2 stretching modes is observed

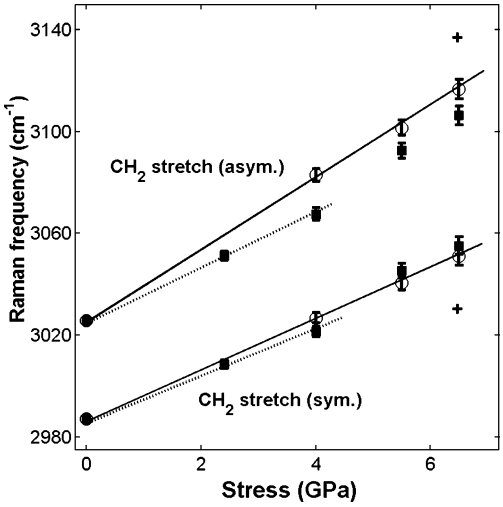

Figure 9. Stress dependence of the Raman frequency for the CH_2 stretching modes, 2987 cm^{-1} (symmetric) and 3026 cm^{-1} (asymmetric), for the [100] orientation (open circles) and the [110] orientation (solid squares). The solid lines show a linear shift with stress for the [100] orientation. The dotted lines denote the shifts up to 4 GPa for the [110] orientation. The crosses denote the frequency of the small peaks shown in lower panel of Figure 8.

above 4 GPa for the [110] orientation only (Figure 9), (iii) large broadening is observed for the CH_2 and NO_2 asymmetric stretching modes for stresses above 4 GPa for the [110] orientation (Figures 3 and 4), and (iv) fitting the CH_2 modes for the [110] orientation requires additional peaks compared to the [100] data (Figure 8). These orientation-dependent results are a consequence of the differences in the microscopic-level response of the PETN crystals to shock compression along the [100] and [110] orientations. To understand the spectroscopic features listed above, a number of possible microscopic-level changes can be considered. However, since previous work[6,8,9] has pointed out the susceptibility of PETN molecules to conformational changes, it is of interest to examine our spectroscopic results to see if the orientation dependence observed can be related to microscopic features associated with the previously proposed conformational changes.

The observed difference in the slopes for the stress-dependent frequency shifts (CH_2 and NO_2 stretching modes) for the [100] and [110] orientations suggests that the PETN molecules respond differently for uniaxial strain along the two crystal orientations, despite the fact that the macroscopic compressibility along the two orientations is similar.[21] These two aspects of the PETN response, one at the molecular level and one at the macroscopic level, can be reconciled by recognizing that the intermolecular interactions across the slip planes are believed[3,6] to be quite different for shock wave compression along the [100] and [110] orientations. Therefore, the anisotropy in our Raman data reflects differences in the details of molecular interactions (and related microscopic deformations) when HE crystals are shock compressed along different crystallographic directions. Also, the significant orientation dependence for the CH_2 and NO_2 stretching modes suggests that the periphery of the molecule is strongly affected by differences in molecular interactions arising from the directionality of the shock compression.

Perhaps the most significant feature of our results is the broadening of certain Raman peaks. This broadening is clearly observed for the asymmetric NO_2 stretching mode and the symmetric and asymmetric CH_2 stretching modes, with the [110] orientation yielding substantially larger broadening than the [100] orientation. In contrast, the NO_2 symmetric stretching

mode showed minimal broadening for both orientations. This broadening behavior for the NO_2 modes under [110] compression closely resembles that observed for PETN in solution.[8] As discussed in ref 8, PETN molecules are believed to assume a variety of different conformations in solution. Thus, the broadening behavior of the NO_2 modes in our experiments is suggestive of conformational changes taking place during shock compression along the [110] orientation. Broadening of the CH_2 modes (Figure 8) provides further evidence for conformational changes under shock loading along the [110] direction. Although clear splitting was not observed in our spectra for the CH_2 modes, comparison with static high-pressure spectra[8,9] (where splitting was observed) suggests that similar changes in the molecular structure likely occur during shock compression, i.e., lowering the molecular symmetry in the crystal. As shown in Figure 8, the highly broadened peaks for the CH_2 symmetric and asymmetric stretching modes at 6.5 GPa for the [110] orientation could not be fitted with just two spectral components; the appearance of new peaks provides support for conformational changes for this orientation.

The discontinuity in the slope of the frequency shifts for the CH_2 stretching modes for the [110] orientation is not as easy to understand, given the lack of any such discontinuity for the NO_2 modes. However, we note that the shock stresses at which the discontinuity occurs correspond to the stresses where anomalous sensitivity to shock-induced chemical reaction was observed for the [110] orientation.[2,4,7] Anomalous spectral features (slope discontinuities and peak splitting) were also observed in the same stress range under hydrostatic loading conditions.[9] The spectral features observed under hydrostatic loading were related to the lowering of molecular symmetry due to conformational changes.

V. Summary and Conclusions

Using single-pulse Raman spectroscopy, developed to provide higher spectral resolution and rejection of background emission, selected vibrational modes were examined to investigate the molecular-level response of PETN single crystals shocked along the [110] (sensitive) and the [100] (insensitive) orientations. The shock-induced frequency shifts for the CH_2 and NO_2 stretching modes showed significant anisotropy (or orientation dependence), while the shifts for the modes corresponding to the interior region of the molecule showed no discernible differences for the two orientations. Also, the CH_2 stretching modes showed a discontinuity in the frequency shift above 4 GPa for [110] compression, corresponding to the stress level associated with the anomalous sensitivity for this orientation.[2,4,7]

The peaks for the CH_2 (symmetric and asymmetric) and NO_2 (asymmetric) stretching modes showed large broadening above 4 GPa for [110] compression; additional peaks, likely due to symmetry changes, are required to fit the CH_2 modes. The large broadening of these peaks is consistent with the results from previous work,[8,9] where similar features were associated with changes in molecular conformation. Thus, the present results provide support for conformational changes in PETN crystals shocked along the [110] orientation.[6]

This work and our previous studies[6−10] were motivated by the following overall objective: to understand the molecular mechanism(s) that govern the anisotropic sensitivity of shocked PETN single crystals.[1−4] The present results have demonstrated significant anisotropy in the Raman spectra. Shock compression along the [110] (sensitive) orientation results in changes in the molecular response that are quite different from the changes observed for compression along the [100] (insensitive) orientation. Although clear splitting in certain vibrational modes, corresponding to changes in molecular conformations, was not observed in our [110] data, analysis of the line broadening data makes a good case for molecular symmetry changes expected from conformational changes.[6,8,9] The combination of theoretical work,[6,10] shock-induced emission results,[7] static high-pressure studies,[8,9] and the present work has provided a reasonably consistent and comprehensive description of the molecular mechanism governing the mechanochemistry in shocked PETN single crystals. Local lattice polarization due to changes in molecular conformations provides the key link between shock compression and onset of chemical decomposition in PETN.[6] Realistic ab initio calculations corresponding to the deformation conditions under shock wave compression would constitute a logical next step.

Acknowledgment. The authors thank Dr. J. J. Dick for providing the PETN crystals and for useful discussions. G. Chantler and K. Zimmerman are thanked for assistance with the experiments. Drs. W. F. Perger and J. R. Asay are acknowledged for useful discussions and comments. This work was supported by ONR MURI grant N00014-01-1-0802 and DOE grant DEFG0397SF21388.

References and Notes

(1) Dick, J. J. *Appl. Phys. Lett.* **1984**, *44*, 859.
(2) Dick, J. J.; Mulford, R. N.; Spencer, W. J.; Pettit, D. R.; Garcia, E.; Shaw, D. C. *J. Appl. Phys.* **1991**, *70*, 3572.
(3) Dick, J. J.; Ritchie, J. P. *J. Appl. Phys.* **1994**, *76*, 2726.
(4) Dick, J. J. *J. Appl. Phys.* **1997**, *81*, 601.
(5) Yoo, C. S.; Holmes, N. C.; Souers, P. C.; Wu, C. J.; Ree, F. H.; Dick, J. J. *J. Appl. Phys.* **2000**, *88*, 70.
(6) Gruzdkov, Y. A.; Gupta, Y. M. *J. Phys. Chem. A* **2000**, *104*, 11169.
(7) Dreger, Z. A.; Gruzdkov, Y. A.; Gupta, Y. M.; Dick, J. J. *J. Phys. Chem. B* **2002**, *106*, 247.
(8) Gruzdkov, Y. A.; Dreger, Z. A.; Gupta, Y. M. *J. Phys. Chem. A* **2004**, *108*, 6216.
(9) Dreger, Z. A.; Gruzdkov, Y. A.; Gupta, Y. M. Manuscript in preparation.
(10) Gruzdkov, Y. A.; Gupta, Y. M. *J. Phys. Chem. A* **2001**, *105*, 6197.
(11) Trott, W. M.; Renlund, A. M. *J. Phys. Chem.* **1988**, *92*, 5921.
(12) Moore, D. S.; Schmidt, S. C.; Shaw, M. S.; Johnson, J. D. *J. Chem. Phys.* **1989**, *90*, 1368.
(13) Pangilinan, G. I.; Gupta, Y. M. *J. Phys. Chem.* **1994**, *98*, 4522.
(14) Tas, G.; Franken, J.; Hambir, S. A.; Hare, D. E.; Dlott, D. D. *Phys. Rev. Lett.* **1997**, *78*, 4585.
(15) Kobayashi, T.; Sekine, T.; He, H. *J. Chem. Phys.* **2001**, *115*, 10753.
(16) Spitzer, D.; Samirant, M. *Tenth Symposium on Detonation*; Office of Naval Research: Arlington, VA, 1993; p 831.
(17) Fowles, G. R.; Duvall, G. E.; Asay, J.; Bellamy, P.; Feistmann, F.; Grady, D.; Michaels, T.; Mitchell, R. *Rev. Sci. Instrum.* **1970**, *41*, 984.
(18) Gupta, Y. M. COPS code; Stanford Research Institute, Menlo Park, CA, 1976, unpublished.
(19) Hemmi, N.; Gupta, Y. M. Manuscript in preparation.
(20) Hemley, R. J. *High Pressure Res. Miner. Phys.* **1987**, 347.
(21) Winey, J. M.; Gupta, Y. M. *J. Appl. Phys.* **2001**, *90*, 1669.